# Simulating the Landau-Zener transitions and Landau-Zener-Stückelberg interferometers with compacted optical waveguides: An invariant method

Hongying Liu,[1] Maochun Dai,[1] and L. F. Wei[1,2,*]

[1]*Information Quantum Technology Laboratory, School of Information Science and Technology, Southwest Jiaotong University, Chengdu 610031, China*

[2]*Photonics Laboratory, Institute of Functional Materials, College of Science, Donghua University, Shanghai 201620, China*

(Received 3 August 2018; published 11 January 2019; corrected 1 March 2019)

Experimental demonstrations of coherent dynamics for the driven quantum system are usually limited by their shorter coherent times (due to the inevitable environment noises). Given the Maxwell equation for the electromagnetic waves (EMWs) prorogating in the optical waveguides takes the similar form of the Schrödinger equation for the driven quantum system, the quantum dynamics in time domain can be simulated by the light propagating along the waveguide in spatial domain. To simulate the fast time evolutions of quantum states during the Landau-Zener (LZ) transitions and Landau-Zenner-Stückelberg (LZS) interferences for the periodically driven two-level systems, we develop an invariant method to design the compacted curved wavguides and demonstrate the LZ transitions and LZS interferometery in the spatial domain. Due to significantly long coherent lengths of the EMWs propagating along the waveguides, the proposed optical-quantum analogies should be feasible with the current integrated optical devices.

DOI: 10.1103/PhysRevA.99.013820

## I. INTRODUCTION

Quantum transition and quantum interference as two typical coherent effects in quantum mechanics, which have been successfully utilized to explain many phenomena in chemistry and physics. Specifically, the Landau-Zener (LZ) transitions [1–3], served usually as one of the simplest but the most fundamental evidences to experimentally confirm the quantum cherence in a driven quantum system. It is demonstrated with, Rydberg atoms [4], field-driven superlattices [5], and superconducting circuits [6], etc. Physically, one of the most challenges to experimentally demonstrate the LZ transitions as well as the further Landau-Zenner-Stückelberg (LZS) interference [7] is that the coherent time of the driven quantum system is practically limited due to various inevitable environment noises.

Quantum-optical analogy, i.e., simulating the quantum coherence phenomena in the driven quantum systems in the time domain with the EMWs propagating along certain optical waveguide structures in the spatial domain, has been given much attention in the recent years [8]. The reason is that the Maxwell equation on the EMWs propagating along the curved optical waveguides is formally equivalent to the Schrödinger equation on the dynamics for a driven quantum system. As a consequence, the intensity distributions of the electromagnetic field in the waveguides take the analogous roles of the population distributions of the quantum states in the relevant quantum dynamics. Furthermore, the interwaveguide interactions are analogous to the interactions between the quantum states. Given the spatial optical coherence is more robust than the time quantum coherence in the usual room-temperature environment [9,10], various quantum coherence evolutions in the time domain can be roust demonstrated with the spatial distributions of the EMWs in the corresponding optical waveguides. In fact, these quantum-optical analogies have delivered certain interesting applications, typically, e.g., demonstrating the Bolch oscillations, coherent population transfers, coherent control of quantum tunnelings, etc. [11–22], with certain integrated optical devices [23–25]. In our recent work [26], we studied the fundamental quantum logic gates in the spatial domain with the coupled three-waveguide devices. Therefore, the application of the quantum-optical analogy to simulate various fast evolving quantum coherent phenomena are particularly expected.

Certainly, the first task for the implementations of the desirable quantum-optical analogies is to design the relevant waveguide structures. However, this is not easy as the coupled-mode equations for the light prorogations in the desired curved waveguides are usually solved numerically. Also, due to the practical limitations of the spatial scales in the integrated optics, the compacted waveguide structures are particularly desirable. Given the Lewis-Riesenfeld (LR) invariant method [27] have been successfully applied to solve the time-domain quantum dynamical problem for various driven quantum systems and have been utilized to design the desired fast evolution paths of quantum states [28]. In this paper we generalize such a technique to investigate the problem of the light propagations in the waveguides in the spatial domain. With this technique the coupled-mode equation for the coupled curved waveguides could be solved analytically, instead pure numerically. As a consequence, inversely designing various compact wavguide structures to simulate various time-domain quantum coherent dynamics with the feasible integrated optical devices in spatial domain could be implemented. Specifically, to implement the quantum-optical

*lfwei@mail.swjtu.edu.cn

 

analogies of the periodically driven LZ dynamics and the LZS interference, we use the invariant method to solve the relevant coupled-mode equations for the two coupled curved waveguides and then properly design the interwaveguide coupling parameters to control the intensity distributions of electromagnetic field in the two waveguides. As a consequence, the fast temporal evolutions of the quantum states in the LZ transitions and the LZS interferometery are simulated by the spatial propagations of the light along the compacted curved waveguides.

The rest of this paper is organized as follows. In Sec. II, after briefly reviewing the standard LZ formula, we use the LR invariant method to exactly solve the LZ problem with the linear driving and demonstrate the LZS interferometry with a two-state quantum system under the periodic driving. In Sec. III, by making use of the analogy between the spatial-domain coupled-mode equation in curved waveguides and the time-domain Schrödinger equation for the driven two-state quantum system, we develop a spatial-domain invariant method to exactly solving the Maxwell equation for the light propagating along the curved waveguides and then design the compacted waveguide devices to demonstrate the LZ transitions and the LZS interferometry in spatial domains. Finally, conclusions and discussions are given in Sec. IV.

## II. INVARIANT METHOD TO EXACTLY SOLVE THE QUANTUM DYNAMICS OF A DRIVEN TWO-LEVEL SYSTEM

Originally, Landau and Zener considered the quantum dynamical problem describing by the time-dependent Schrödinger equation ($\hbar \equiv 1$),

$$i\frac{\partial|\psi(t)\rangle}{\partial t} = H(t)|\psi(t)\rangle, \quad H(t) = \frac{\varepsilon(t)}{2}\sigma_z + \frac{\Delta_0}{2}\sigma_x. \tag{1}$$

Here, $\sigma_z$ and $\sigma_x$ are the relevant Pauli operators, $\Delta_0$ is a constant, and $\varepsilon(t) = \nu t$ (with $\nu$ being a constant) the linearly time-dependent driving. Obviously, the generic solution of the LZ problem could be expressed as $|\psi(t)\rangle = b_1(t)|1\rangle + b_2(t)|2\rangle$ with $|1\rangle \equiv (0,-1)^T$ and $|2\rangle \equiv (1,0)^T$ being the two so-called diabatic states with the energies $\nu t$. The basic task in this problem is to investigate how the populations: $|b_1(t)|^2$ and $|b_2(t)|^2$ of these diabatic states evolve under the applied linear driving.

As sketched in Fig. 1, the adiabatic eigenvalues,

$$e_\pm(t) = \pm\tfrac{1}{2}\sqrt{(\nu t)^2 + \Delta_0^2}, \tag{2}$$

of the time-dependent Hamilatonian $H(t)$ possesses an avoided crossing at the point $t = 0$ for $\Delta_0 \neq 0$. Under the adiabatic limit, $\nu \ll \Delta_0^2$, i.e., the sweep occurs slowly enough, the system evolves along the adiabatic paths (the solid lines in Fig. 1), and the populations of the diabatic states will be exchanged, e.g., the system in state $|1\rangle$ prepared at $t = -\infty$ will evolve slowly into state $|2\rangle$. Certainly, if the sweep is not sufficiently slow and thus the adiabatic condition is broken, then the transitions could be occurred between the adiabatic state. For example, if at time $t = -\infty$ the system is prepared in state $|1\rangle$, i.e., $|\psi(-\infty)\rangle = |1\rangle$, then the final probability $P_{\rm LZ}$ that the atom ends up in state $|1\rangle$, i.e., $|\psi(+\infty)\rangle = |1\rangle$ is given

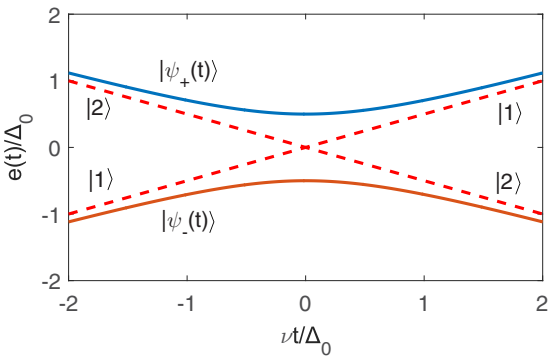


FIG. 1. Energy levels of a linearly driven two-level system versus the driving time. Here, the dashed line corresponds to the case of $\Delta_0 = 0$, and an avoided crossing exists at $t = 0$ for the case with $\Delta_0 \neq 0$. Diabatic states: $|1\rangle$, $|2\rangle$, adiabatic states: $|\psi_\pm(t)\rangle$.

by [1,2]

$$P_{\rm LZ} = \exp\left[-\frac{\pi\Delta_0^2}{2\nu}\right]. \tag{3}$$

This is the famous LZ formula (LZF). In the limit $\Delta_0 \to 0$, $P \to 1$, the crossing is said to be traversed diabatically. Inversely, when $\Delta_0 \gg \nu$, $P \to 0$, the avoided crossing is said to be traversed adiabatically. Obviously, quantum coherence should be kept during the transitions. Thus, experimentally observing such tunneling could be served as the robust evidence of the quantum coherence in such a driven two-state quantum system. In practicality, LZ transitions are not easy to be observed experimentally due to the fact that coherence times of most driven quantum systems are typically short. In fact, the quantum tunnelings near the avoid-crossing point is very complicated and cannot be described by the LZ formula. Below, we solve such a problem by the LR dynamical invariant method to exactly determine the occupation probabilities of the states at any time for arbitrary driving parameters.

### A. Solving the LZ problem with the LR invariant theory

Based on the LR invariant theory [27], the generic solution to the time-dependent Schrödinger equation (1) can be constructed as

$$|\psi(t)\rangle = \sum_n u_n e^{j\alpha_n}|\phi_n(t)\rangle. \tag{4}$$

Here, $|\phi_n(t)\rangle$ being the instantaneous eigenstates of the dynamical invariant $I(t)$, which is determined by the equation,

$$i\frac{\partial I(t)}{\partial t} = [H(t), I(t)], \tag{5}$$

with $u_n$ being the time-independent superposition coefficients and $\alpha_n(t) = \int_0^t \langle\phi_n(t')|i\partial/\partial t' - H(t')|\phi_n(t')\rangle dt'$ the so-called Lewis-Riesenfeld phase [28]. For a generic two-state-driven quantum system, its Hamiltonian $H(t)$ can be generically written as

$$H(t) = \frac{1}{2}\begin{bmatrix}\varepsilon(t) & \Delta(t)\\ \Delta(t) & -\varepsilon(t)\end{bmatrix}, \tag{6}$$

in the basis $\{|1\rangle \equiv (0,-1)^T, |2\rangle \equiv (1,0)^T\}$. Above, $\varepsilon(t)$ and $\Delta(t)$ are the time-dependent detuning and Rabi frequency, respectively. The instantaneous eigenstates of the Hamiltonian (6), corresponding to the time-dependent eigenvalues: $e_\pm(t) = \pm\sqrt{\varepsilon^2(t) + \Delta^2(t)}/2$, read

$$|\psi_+\rangle = \begin{bmatrix} \cos\frac{\sigma(t)}{2} \\ \sin\frac{\sigma(t)}{2} \end{bmatrix}, \quad |\psi_-\rangle = \begin{bmatrix} \sin\frac{\sigma(t)}{2} \\ -\cos\frac{\sigma(t)}{2} \end{bmatrix}, \tag{7}$$

with $\tan\sigma(t) = \Delta(t)/\varepsilon(t)$. A dynamical invariant, corresponding to the generic Hamiltonian (6), can be constructed as [28]

$$I(t) = \frac{\mu}{2}\begin{bmatrix} \cos\gamma & \sin\gamma e^{i\theta} \\ \sin\gamma e^{-i\theta} & -\cos\gamma \end{bmatrix}, \tag{8}$$

where $\mu$ is an arbitrary constant with the unit of frequency for keeping $I(t)$ possesses the dimension of the energy. The parameters $\gamma$ and $\theta$ are determined by

$$\frac{d\gamma}{dt} = \Delta(t)\sin\theta, \tag{9}$$

and

$$\frac{d\theta}{dt} = \Delta(t)\cot\gamma\cos\theta - \varepsilon(t). \tag{10}$$

Obviously, the instantaneous eigenstates of the invariant operator $I(t)$ in Eq. (8) read

$$|\phi_+(t)\rangle = \begin{bmatrix} \cos\frac{\gamma}{2}e^{i\theta} \\ \sin\frac{\gamma}{2} \end{bmatrix}, \quad |\phi_-(t)\rangle = \begin{bmatrix} \sin\frac{\gamma}{2} \\ -\cos\frac{\gamma}{2}e^{-i\theta} \end{bmatrix}, \tag{11}$$

corresponding to the eigenvalues $\lambda_\pm = \pm\mu/2$. Consequently, Eq. (4) becomes

$$|\psi(t)\rangle = \sum_{n=+,-} u_n \exp[i\alpha_n(t)]|\phi_n(t)\rangle, \tag{12}$$

with $u_\pm = e^{-i\alpha_\pm(t_0)}\langle\phi_\pm(t_0)|\psi(t_0)\rangle$, and

$$\alpha_\pm(t) = \pm\int_{t_0}^{t}\left(\dot\theta + \frac{\dot\gamma\cot\theta}{\sin\gamma}\right)dt'. \tag{13}$$

where $t_0$ is the start time of the evolution.

Next, the trajectory of the state evolutions can be parametrized according to the eigenstates $|\phi_k(t)\rangle$. Specifically, with the initial condition [28] $\gamma(t_0) = 0$, we can get the $t$-independent superposition coefficients,

$$u_+ = 0, \quad u_- = e^{i\theta(t_0)}e^{-i\alpha_-(t_0)}. \tag{14}$$

Substituting Eqs. (11), (13) and (14) into Eq. (12), the populations $|b_1(t)|^2$ and $|b_2(t)|^2$ of the diabatic states $|1\rangle$ and $|2\rangle$ are given by

$$P_1(t) = |b_1(t)|^2 = |\langle 1|\psi(t)\rangle|^2 = \cos^2\left(\frac{\gamma}{2}\right), \tag{15}$$

and

$$P_2(t) = |b_2(t)|^2 = |\langle 2|\psi(t)\rangle|^2 = \sin^2\left(\frac{\gamma}{2}\right), \tag{16}$$

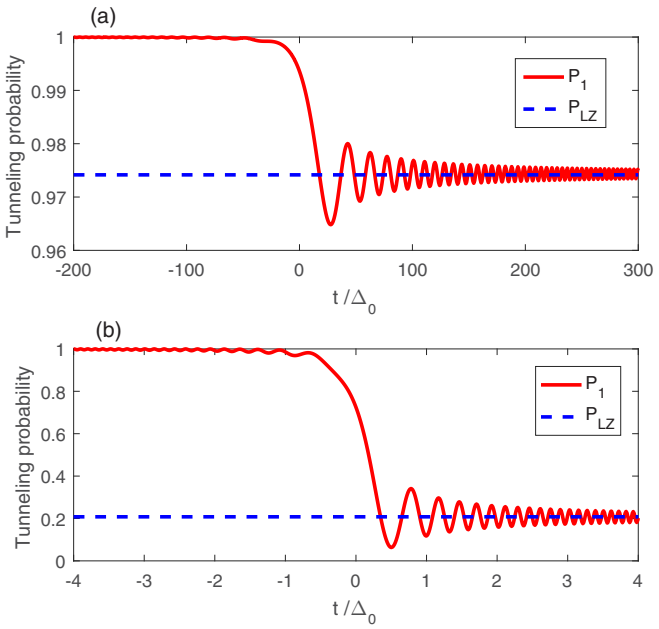


FIG. 2. The time-dependent LZ transition probability in a driven two-level system with the Hamiltonian $H(t)$ for the initial state $|\psi(-\infty)\rangle = |1\rangle$. The red solid line represents the time-dependent probability for the system staying at state $|1\rangle$, and the blue dashed line shows the asymptotic occupation probability $|1\rangle$ calculated by the LZF. Here, the relevant parameters are set as: (a) $\Delta_0 = 0.1$ and $\nu = 0.6$, (b) $\Delta_0 = 2$ and $\nu = 4$, respectively.

respectively. Thus, once the driving parameters $\Delta(t)$ and $\varepsilon(t)$ are given the time evolutions of the occupation probabilities of states $|1\rangle$ and $|2\rangle$ can be determined exactly. As a consequence, how the LZ transitions across the avoid point can be exactly investigated.

The original LZ model corresponds to the situation, wherein $\varepsilon(t) = \nu t$ and $\Delta(t) = \Delta_0$, i.e., the Rabi pulse is constant, but the Stark pulse changes linearly with the time. This problem has been discussed widely [3]. In Fig. 2 we show the time-dependent occupation probabilities: $P_1(t)$ of states $|1\rangle$ (the solid lines) with the initial condition $|\psi(-\infty)\rangle = |1\rangle$ for different driving parameters (a) $\Delta_0 = 0.1$ and $\nu = 0.6$ and (b) $\Delta_0 = 2$ and $\nu = 4$. It is seen that, after the sufficiently long evolution time, the diabatic transition probability agrees well with the results predicted by the LZF, shown as the blue dashed lines in Fig. 2.

### B. Time-domain LZS interferometry based on the dynamical invariant solutions

We now treat the dynamics of a two-level quantum system under the driving of a large-amplitude periodic external field. For simplicity, we assume that the Rabi pulse is time independent, i.e., $\Delta(t) = \Delta_1$, but the Stark pulse is a periodic function, i.e.,

$$\varepsilon(t) = \varepsilon_0 + E\cos(\Omega t). \tag{17}$$

This problem had been investigated mainly by two approaches [7,29]: The discretized adiabatic transfer matrix (TM) approaches and the rotating-wave approximation (RWA). They

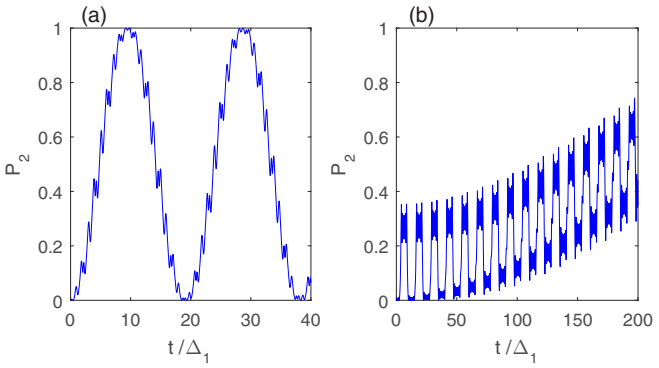


FIG. 3. The occupation probability $P_2$ of state $|2\rangle$ as a function of time $t$, assuming that the system was initially in state $|1\rangle$. Here, the relevant parameters are set as [25] $\Delta_1 = 1$, but (a) $\varepsilon_0/\Delta_1 = 3$, $\Omega/\Delta_1 = 3$, $E/\Delta_1 = 15$, and (b) $\varepsilon_0/\Delta_1 = 1$, $\Omega/\Delta_1 = 0.5$, $E/\Delta_1 = 12$. These results agree well with those by numerically solving the relevant Schrödinger equation.

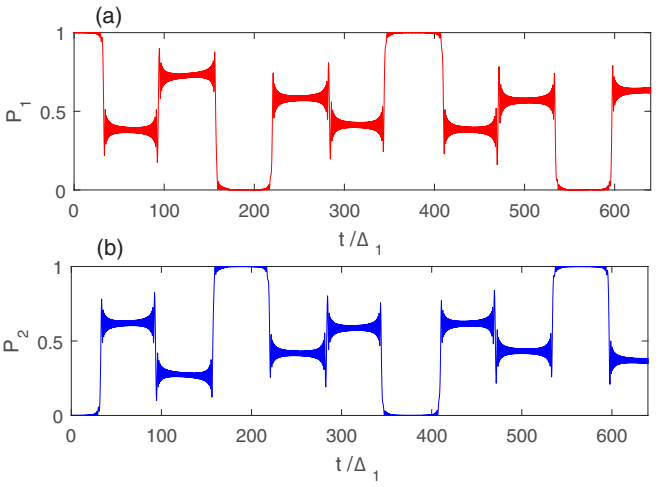


FIG. 4. The occupation probabilities $P_1$ and $P_2$ of states $|2\rangle$ and $|1\rangle$, respectively, as the functions of time $t$ for the initial condition $|\psi(0)\rangle = |1\rangle$. Here, the relevant parameters are typically set as $\Delta_1 = 1$, $\varepsilon_0/\Delta_1 = 1$, $\Omega/\Delta_1 = 0.05$, $E/\Delta_1 = 30$. The occupation probability $P_1(t)$ [or $P_2(t)$] shows the quasiperiodic phenomena due to the quantum interference. Certainly, $P_1(t) + P_2(t) \equiv 1$ for the present system without dissipation.

are, respectively, valid in different parameter regions. Now, the problem is solved uniformly by the LR invariant theory demonstrated above. Our results, i.e., the time-dependent occupation probability $P_2$ of state $|2\rangle$ are shown in Fig. 3 in which sudden jumps correspond to the LZ transitions near the avoid crossing points. It is emphasized that the present results agree well with those by numerically solving the relevant Schrödinger equation in Ref. [29]. In Fig. 3(a) the parameters satisfy the condition $\Omega/\Delta_1 > 1$, and thus it agrees with that by the usual RWA [29]. Note that under the parameter conditions [29] $E/\Delta_1 > 1$ and $E\Omega > \Delta_1^2$, shown in Fig. 3(b), both the TM method and the RWA fail.

In principle, the dynamical invariant method demonstrated above works well for the arbitrary parameter condition of the driving. For example, for the typically selected parameters $\varepsilon_0/\Delta_1 = 1$, $\Omega/\Delta_1 = 0.05$, $E/\Delta_1 = 30$, how the occupation probabilities of states $|1\rangle$ and $|2\rangle$ evolve are shown in Fig. 4 for initial-state $|\psi(0)\rangle = |1\rangle$. Certainly, the sum of all the possible occupation probabilities is always conservation, i.e., $P_1(t) + P_2(t) \equiv 1$, for the present driven two-level system without any dissipation. Note that either the occupation probability $P_1(t)$ or $P_2(t)$ shows the quasiperiodic phenomena [7], which are known as Stückelberg oscillations.

It is shown in Fig. 5 that the instantaneous eigenvalues of the present time-dependent Hamiltonian exist two avoid-crossing points $M$ and $N$ in a period. During the time evolution across point $M$, the initial population of state $|1\rangle$ is split into states $|1\rangle$ and $|2\rangle$. This implies that the relevant LZ transitions at the point act as a beam splitter of the occupations [30]. The probabilities $P_2$ (the probability of staying at the opposite diabatic state of the input state) and $P_1$ (the probability of staying at the same diabatic state of the input state) could be served as the relevant reflection and the transmission coefficients, respectively. These two components are schematically illustrated in Fig. 5 with the trajectories marked by double and single arrows, respectively. After splitting, a relative phase is acquired due to the energy difference between the two states. If the drive $\varepsilon(t)$ sweeps the system through the second avoided crossing point $N$, the quantum state collides and quantum mechanically interferences take place. The cumulative result is a typical quantum state interferometer, and the relevant interference fringes depend on the LZ transition amplitudes and the evoultion phases of the driven quantum states.

Specifically, we show numerically the LZS interference pattern, e.g., the occupation probability $P_2$, depends on the bias offset $\varepsilon_0/\Omega$ and the driving amplitude $E/\Omega$ in Fig. 6 at different evolution times. Certainly, the interference pattern depends on the total relative phase accumulated by the evolution. For simplicity, we assume that the system starts from state $|1\rangle$ and treat $\Omega$ as a fixed parameter. Under the fast-passage limit [31] $E\Omega \gg \Delta_1^2$, e.g., $\Omega/(2\pi) = 1.2$ and $\Delta_1 = 0.004$ GHz, we can see in Fig. 6 that the occupation probability $P_2$ reveals certain displacement and overlap, i.e., interference fringes, after a certain driving time [e.g., shown

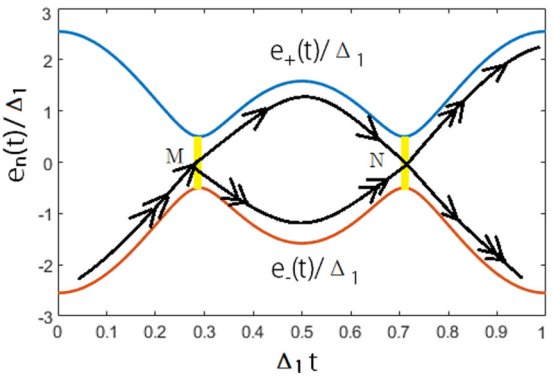


FIG. 5. Time evolution of the energy spectrum during one period. The evolutions of the quantum state traverse two avoided-crossing regions within a period of the driving. Here $e_\pm(t) = \pm\sqrt{\varepsilon^2(t) + \Delta_1^2}/2$, $\varepsilon(t) = \varepsilon_0 + E\cos(\Omega t)$ with $\Delta_1 = 1$, $\varepsilon_0/\Delta_1 = 1$, $E/\Delta_1 = 4$, and $\Omega/\Delta_1 = 2\pi$.

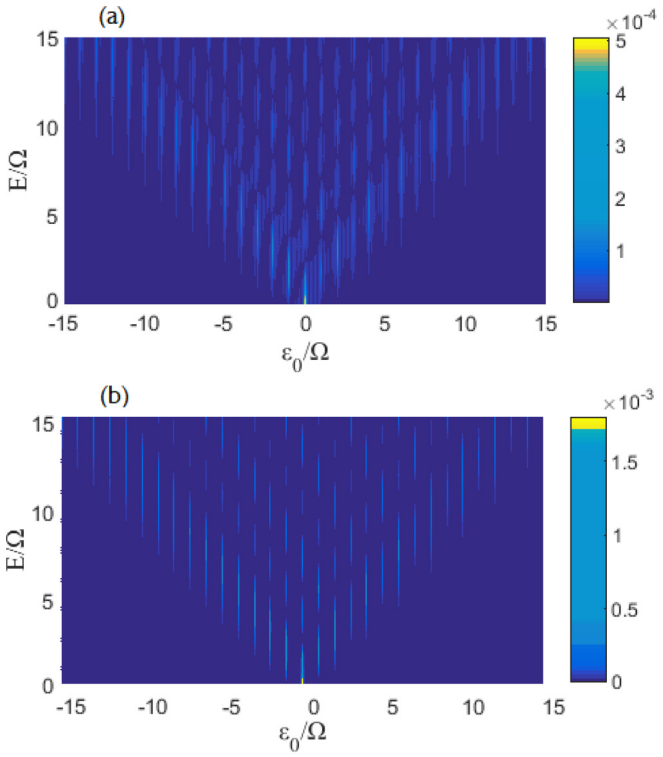


FIG. 6. Time-domain LZS interferometry for $E\Omega \gg \Delta_1^2$: the time-averaged occupation probability $P_2$ of diabatic state $|2\rangle$ versus the bias offset $\varepsilon_0$ and the driving amplitude $E$ for the parameters $\Omega/(2\pi) = 1.2$, $\Delta_1 = 0.004$ GHz. (a) The interference pattern at the evolution time 10 ns, which corresponds to shorter interference time. (b) The interference pattern with a better interference contrast with the higher interference ratio after the longer evolution time, e.g., after 20 ns.

in Fig. 6(a) at 10 ns]. Figure 6(b) shows that with the increase in the evolution time, e.g., after 20 ns, the cascaded LZ transitions lead to a stronger interference and thus show the clearer interference pattern. This agrees well with the relevant experimental results in Ref. [31]. Certainly, if the value of the parameter $E$ is sufficiently smaller than the bias offset $\varepsilon_0$, no LZ transition occurs, and, consequently, the LZS interference pattern does not appear.

## III. SIMULATIONS OF THE LZ-LIKE TRANSITIONS AND LZS-TYPE INTERFEROMETRY WITH CURVED WAVGUIDES IN SPATIAL DOMAINS

The most obstacle to experimentally demonstrate the time-domain LZ transitions and LZS interferences is the finite coherent time of the driven quantum system. Expectedly, the significantly long coherent path for the light coherently propagating along the optical waveguide could be utilized to implement the quantum interferences in the spatial domain. Below, we show how the optical analogies of the LZ transitions and the LZS interferometry could be implemented with the curved waveguides wherein the interwaveguide coupling can be designed precisely.

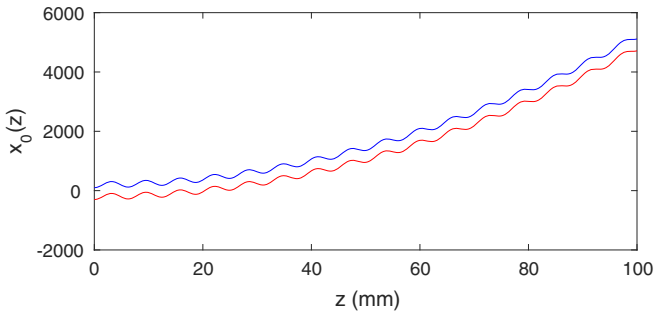


FIG. 7. Schematic of a cosine curved directional coupler, the related parameters are as follows: $\Delta\beta = 1\ \mathrm{mm}^{-1}$, $q_0/\Delta\beta = 1$, $\omega/\Delta\beta = 1$, $A/\Delta\beta = 100$.

### A. Exactly solving the coupled-mode equation of the curved waveguides by the invariant method

We consider the propagations of the monochromatic light waves of the wavelength $\lambda$ (in vacuum) along a curved coupled-waveguide structure, shown in Fig. 7. In the scalar and paraxial approximations, the electric-field amplitude in the waveguides can be written as $\Psi(x, y, z, t) = \psi(x, y, z)\exp[i(kn_s z - \omega t) + \text{c.c.}]$ with $n_s$ being the refractive index of the substrate and $\omega = kc_0$. $\psi(x, y, z)$ is the slow-varying field envelope satisfying the paraxial wave equation,

$$i\hbar\frac{\partial\psi}{\partial z} = -\frac{\hbar^2}{2n_s}\nabla_x^2\psi + V[x - x_0(z)]\psi. \tag{18}$$

Here, $x_0(z)$ is the axis bending profile, $z$ is the paraxial propagation distance, $\hbar = \lambda/2\pi = 1/k$ is the reduced wavelength, and $V(x) = [n_s^2 - n^2(x, y)]/(2n_s) \simeq n_s - n(x, y)$ with $n(x, y)$ being the refractive index profile of the guiding structure. For simplicity, we assume that the directional coupler is made of two identical waveguides (of length $L$) separated by the distance $a$ in the transverse $x$ direction. In a new reference frame,

$$x' = x - x_0(z), \tag{19}$$

we have

$$\phi(x', z) = \psi(x', z)\exp[-i(n_s/\hbar)\dot{x}_0(z)x' - i\varphi(z)], \tag{20}$$

with $\dot{x}_0(z) = dx_0(z)/dz$ and $\varphi(z) = (n_s/2\hbar)\int_0^z d\xi\ \dot{x}_0^2(\xi)$. Substituting Eqs. (19) and (20) into Eq. (18), we have

$$i\hbar\frac{\partial\phi}{\partial z} = \left[-\frac{\hbar^2}{2n_s}\nabla_x^2 + V(x') + S(z)x'\right]\phi, \tag{21}$$

where $S(z) = n_s d^2x_0/dz^2$. Obviously, if the spatial variable $z$ is replaced by the temporal variable $t$ and $n_s$ is replaced by the mass $m$, Eq. (21) describes nothing but the Schrödinger equation for a particle (with mass $m$) being trapped in a one-dimensional bistable double-well potential $V(x')$ and subjected by an external driving field $S(z)$.

Without the driving field, the eigenmode functions $\xi_1(x')$ and $\xi_2(x')$ of the coupled waveguides are determined by the equation [8],

$$-\frac{\hbar}{2n_s}\frac{\partial^2\xi_{1,2}(x')}{\partial x'^2} + V(x')\xi_{1,2}(x') = \hbar\beta_{1,2}\xi_{1,2}(x'), \tag{22}$$

where the functions $\xi_1(x') = |\xi_1\rangle = \frac{1}{\sqrt{2}}(1,1)^T$ and $\xi_2(x') = |\xi_2\rangle = \frac{1}{\sqrt{2}}(-1,1)^T$ are orthogonal and normalized, i.e., $\langle\xi_1|\xi_1\rangle = \langle\xi_2|\xi_2\rangle = 1$ and $\langle\xi_1|\xi_2\rangle = 0$. $\beta_1$ and $\beta_2$ are nearly degenerate propagation constants. Without loss of generality, the two waveguides are assumed to be identical, and thus, $V(x)$ turns out to be a symmetric function of $x$, i.e., $V(x') = V(-x')$. Also, $\xi_{1,2}(x')$ are real and possess the opposite parties. Phenomenologically, the combinations $f_{1,2}(x') = [\xi_1(x') \pm \xi_2(x')]/\sqrt{2}$ correspond to the light beam distributions in the two waveguide. The shift parameter $\Delta\beta = (\beta_1 - \beta_2)/2$ is responsible to the optical coupling between the waveguides. Neglecting the excitation of the radiation modes, $\phi(x', z)$ can be rewritten as

$$\phi(x', z) = [C_1(z) f_1(x') + C_2(z) f_2(x')] e^{-i\beta_a z}, \tag{23}$$

where $C_l(z)$, $l = 1, 2$ is the amplitude of the light waves trapped in the $l$th waveguide and $\beta_a = (\beta_1 + \beta_2)/2$. Due to the symmetry $\langle\xi_1|x'|\xi_1\rangle = \langle\xi_2|x'|\xi_2\rangle = 0$, Eqs. (21) and (23) reduce [12]

$$i\frac{\partial C_1}{\partial z} = \Delta\beta\, C_2 + \frac{\langle\xi_1|x'|\xi_2\rangle}{\hbar} S(z) C_1, \tag{24}$$

and

$$i\frac{\partial C_2}{\partial z} = \Delta\beta\, C_1 - \frac{\langle\xi_1|x'|\xi_2\rangle}{\hbar} S(z) C_2, \tag{25}$$

respectively. Under the approximation $\langle\xi_1|x'|\xi_2\rangle \simeq a/2$, we have

$$i\frac{d}{dz}\begin{bmatrix} C_1 \\ C_2 \end{bmatrix} = H(z)\begin{bmatrix} C_1 \\ C_2 \end{bmatrix}, \quad H(z) = \begin{bmatrix} F(z) & \Delta\beta \\ \Delta\beta & -F(z) \end{bmatrix}, \tag{26}$$

with $F(z) = aS(z)/(2\hbar)$. This is the spatial-domain version of the dynamics for a driven two-level quantum system discussed above.

Analogously, the spatial-domain dynamical equation (26) can also be exactly solved by using the generalized LR invariant method in which the spatial-domain invariant $I(z)$ is determined by

$$I(z) = \frac{E_0}{2}\begin{bmatrix} \cos\gamma & \sin\gamma e^{i\theta} \\ \sin\gamma e^{-i\theta} & -\cos\gamma \end{bmatrix}, \tag{27}$$

with

$$\frac{d\gamma}{dz} = 2\,\Delta\beta\,\sin\theta, \tag{28}$$

and

$$\frac{d\theta}{dz} = 2\,\Delta\beta\,\cot\gamma\,\cos\theta - 2F(z), \tag{29}$$

satisfying the condition,

$$i\frac{dI(z)}{dz} = [H(z), I(z)]. \tag{30}$$

As a consequence, by using the LR method demonstrated above for the time-domain problem, the intensities of the light distributed in the waveguides after the prorogating distance $z$ can be calculated as

$$|C_1(z)|^2 = \cos^2\left(\frac{\gamma}{2}\right), \quad |C_2(z)|^2 = \sin^2\left(\frac{\gamma}{2}\right). \tag{31}$$

As we mentioned, the coupled-mode equation for the light propagating along the coupled-waveguide system is formally equivalent to the Schrödinger equation for the driven quantum system. Therefore, the dynamics for a driven quantum system the in time domain can be simulated with the exact solutions to the coupled-mode equation in the spatial domain. For the simulations, the occupancy probabilities of the quantum states are replaced by the intensities of the light in the relevant waveguides. Differing from the previous works to simulate the fast temporal evolution of the quantum-mechanical wave functions of the driven atoms and molecules with the spatial light propagations along various waveguide structures [12,13,15,17,19], here the used coupled waveguides are designed by using the analogous invariant solutions of the coupled-mode equations. Therefore, the desirable waveguide devices to simulate the relevant quantum dynamics in the spatial domain could be designed compactly.

### B. LZ-like transitions in a curved compacted-waveguide structure

Typically, let us consider cubically curved coupled waveguides demonstrated experimentally in Ref. [13], where

$$x_0(z) = \frac{8W}{L^3}(z - L/2)^3, \quad 0 < z < L. \tag{32}$$

Here, $2W$ (with $W \ll L$) is the maximum lateral shift of the waveguide axis. In this case, the diagonal elements of the Hamiltonian $H(z)$ in Eq. (26) was given as

$$F(z) = \nu z, \tag{33}$$

with $\nu \simeq 48\pi a W n_s/(\lambda L^3)$ being the analogy of a fixed sweep rate. This waveguide device has been fabricated with the femtosecond-laser writing technique and used to simulate the original time-domain LZ tunneling process during a finite-coupling duration [13]. We now simulate such a result based on the above invariant solution and show numerically intensity distributions of the light in two waveguides $|C_1(z)|^2$ and $|C_2(z)|^2$ calculated by Eqs. (28)–(31) for the experimental parameters [13] $\nu \approx 0.012\ \text{mm}^{-2}$, $\Delta\beta = 0.063\ \text{mm}^{-1}$. It is seen that our results, shown schematically in Fig. 8, agree well with the experimental observations [13].

Note that the above higher efficiency simulations take the benefits from the invariant solutions (rather than the numerical ones) of the coupled-mode equation and thus could be convenient to design the prorogation paths of the light in the waveguides for the desired device applications. This can be achieved by properly setting the boundary conditions, i.e., the parameters $\theta$ and $\gamma$ at the input port ($z = 0$) and the output one ($z = L$) and, consequently, the desirable waveguide parameters. For example, if we want to implement the transfer of the light intensities between the two waveguides, e.g., the completely transfer from waveguide 1 to waveguide 2.

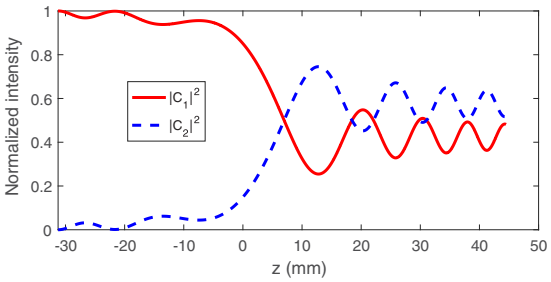


FIG. 8. Intensities of the light in the two waveguides change with the propagating distance $z$; the dashed and solid curves are obtained from Eq. (31) with the relevant parameters being set as $\Delta\beta = 0.063$, $F(z) = 0.012z$ mm$^{-1}$. The simulated LZ-like transitions agree with the relevant experimental observations [13].

Corresponding to the boundary conditions,

$$|C_1(0)|^2 = 1, \quad |C_2(0)|^2 = 0;$$
$$|C_1(L)|^2 = 0, \quad |C_2(L)|^2 = 1, \tag{34}$$

the parameters $\gamma(z)$ in Eqs. (28) and (29) could be designed as

$$\gamma(z) = \gamma_0(z) = \frac{D}{L}z, \tag{35}$$

with $D$ being a $z$-independent adjustable parameter. Meanwhile, by setting simply the $\theta$ parameter as a $z$-independent variable [9,10], such as $\theta = \theta_0 \neq \pi/2$, we get

$$F(z) = F_0(z) = \Delta\beta \cot[\gamma_0(z)] \cos[\theta_0(z)], \tag{36}$$

and

$$\Delta\beta = \frac{D}{2L \sin\theta}, \tag{37}$$

respectively, from Eqs. (28) and (29). Consequently, the condition (34) can be satisfied by simply setting

$$\gamma(L) = D = \pi. \tag{38}$$

Figure 9(a) shows how the designed parameters $F(z)$ and $\Delta\beta$ versus $z$ implement the desirable complete transfer of the light intensity shown in Fig. 9(b), typically with $\theta = \pi/1.98$ and $L = 2$ mm. Obviously, the waveguide coupler for such a simulation could be designed very compactly.

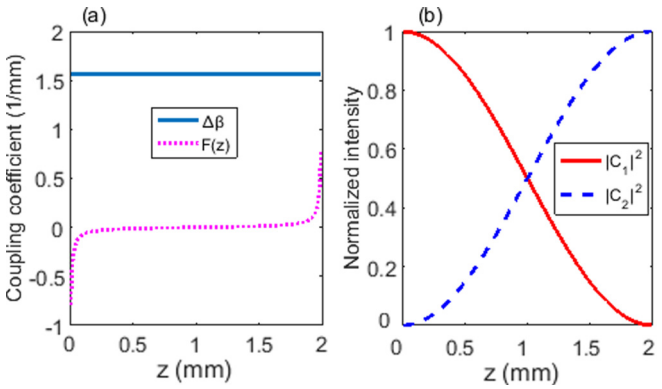


FIG. 9. (a) $z$-dependent coupling coefficients $F(z)$ (dotted curve) and $\Delta\beta$ (solid curve) designed for implementing the light intensity transfer under the boundary conditions, which is numerically realized (b). Here, the relevant parameters are set as $L = 2$ mm, $D = \pi$, and $\theta = \pi/1.98$.

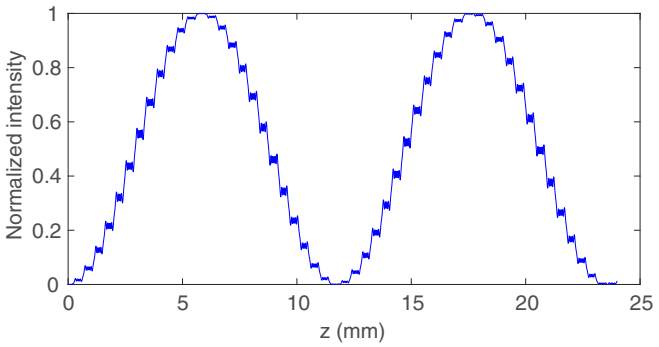


FIG. 10. The distribution of the normalized light intensity $|C_2(z)|^2$ in waveguide 2, and waveguide 1 of the coupler is excited at the input port $z = 0$, i.e., $|C_1(0)|^2 = 1$. The parameters of the coupled curved waveguides are chosen as $\Delta\beta = 2.6$ mm$^{-1}$, $q_0/\Delta\beta = \omega/\Delta\beta = 7/2.6 = 2.6923$, $A/\omega = 15$.

### C. LZS-type interferometry with a compacted curved-waveguide device

Above, we have demonstrated the simulations of the LZ transitions in two curved waveguides with the $z$-dependent linear couplings. In this subsection, we show how the LZS interferometer in a two-level quantum system driven by a large-amplitude periodic external field can be similarly analogized with a cosine curved waveguides coupler. To this end, we consider a cosine curved waveguide shown in Fig. 7 with the axis bending $x_0(z)$ being designed as

$$x_0(z) = \frac{\hbar}{2an_s}\left[q_0 z^2 - \frac{2A}{\omega^2}\cos(\omega z)\right]. \tag{39}$$

As a result, the diagonal element function in matrix (26) reads

$$F(z) = \tfrac{1}{2}[q_0 + A\cos(\omega z)], \quad \omega = 2\pi/\Lambda, \tag{40}$$

with $\Lambda$ and $A$ being the period and amplitude, respectively, of the periodic waveguide in the spatial domain. $q_0$ is a constant. This is the analogy of the Stark pulse (17) applied to periodically drive the two-level quantum system.

Suppose that waveguide 1 of the coupler is excited at the input port $z = 0$, then the light intensities distributing in two waveguides can be calculated by Eq. (31) via solving the parameter equations (28) and (29). Normally, with the parameters [20] $\Delta\beta = 2.6$ mm$^{-1}$, $\omega/\Delta\beta = 7/2.6 = 2.6923$ (which is used analogously to demonstrate the time evolution of a periodically driven two-level quantum system in paper [32]), the light intensity in waveguide 2 along propagation distance $z$ is shown in Fig. 10 where $q_0 = \omega$ [29]. It is shown that the light intensities in the waveguides reveal the obvious oscillating behaviors. A series of quasiperiodic behaviors are originated from the relevant LZS interferences due to the periodic beam splittings of the light intensities passing through the corresponding avoid-crossing points and then being superposed on one of the waveguides.

With periodic dependence of the light intensity on propagation distance shown in Fig. 10, we discuss how the

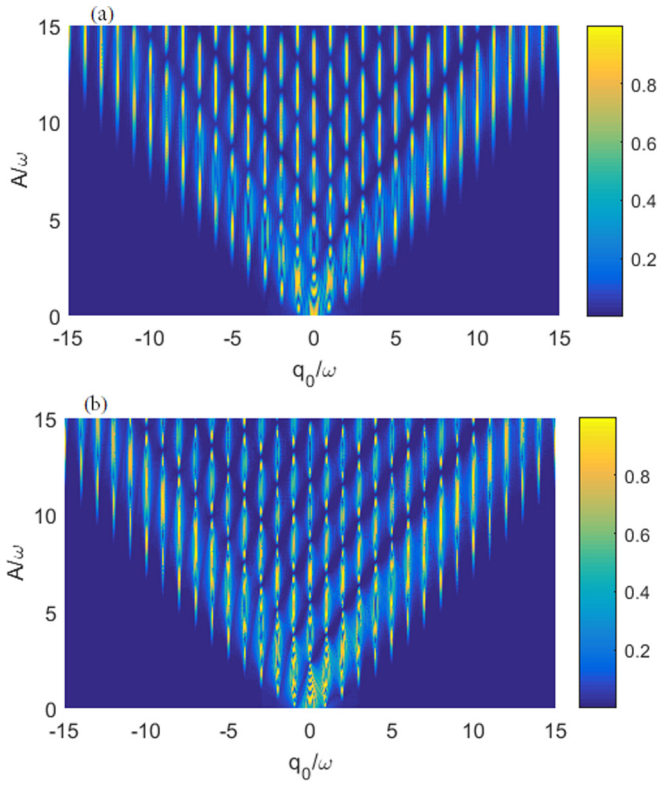


FIG. 11. The spatial-domain version of the LZS interferometry; the normalized light intensity $|C_2(z)|^2$ at certain points versus $A/\omega$ and $q_0/\omega$. The light is assumed to be input along waveguide 1 at $z = 0$ and then propagates to (a) $z = 5.7$ mm and (b) $z = 11.5$ mm. The relevant parameters of the curved waveguides are set as $\Delta\beta = 2.6\ \text{mm}^{-1}$ and $\omega/\Delta\beta = 2.6923$.

$z$-dependent light intensity in waveguide 2 (with $|C_2(0)|^2 = 0$) depending on the other waveguide parameters, i.e., as a function of the waveguide bending amplitude $A/\omega$ and position offset $q_0/\omega$, see Fig. 11 for details. Figure 11 shows more clearly the LZS interference pattern in the spatial domain which depends on $A/\omega$ and $q_0/\omega$ at the propagation distances $z = 5.7$ and $z = 11.5$ mm, respectively. This is the spatial-domain version of the time-domain interference pattern in Ref. [32]. Of course, interference fringes appear at half-integer and integer values of the relative phase.

## IV. DISCUSSION AND CONCLUSION

Given the similarity between the light propagation in wave optics and the quantum dynamics for the driven quantum system, some coherent quantum effects encountered usually in the atoms and molecules can be effectively simulated with the corresponding light propagations in the macroscopic waveguide structure composed of the evanescent couplings. In this paper, in the framework of the invariant method, we uniformly investigated the LZ transition and the LZS interferometry in a driven two-level quantum system and the light propagations along two coupled curved waveguides. It had been demonstrated that the time domain LZ transitions and LZS interferometry in the driven two-level quantum system could be effectively simulated with the intensities of the light propagating along the curved waveguides. Due to the significantly long coherent length of the light propagations along the optical waveguide, the proposed approach is specifically suitable to simulate quantum coherent dynamics, which is not easy to realize in the usual quantum system (due to the inviolable decoherence).

One of the best advantages in the proposed invariant method to simulate quantum coherent dynamics with waveguides in spatial domain is that the relevant optical waveguides can be designed as the desirable compacted structures beyond the usual adiabatic limit. Therefore, it is good for the integrated optics implementations.

## ACKNOWLEDGMENTS

This work was supported by the National Natural Science Foundation of China (NSFC), Grant No. U1330201. We thank also Dr. M. Hussain for useful discussions.

[1] L. D. Landau, Phys. Z. Sowjetunion **2**, 46 (1932).
[2] C. Zener, Proc. R. Soc. London, Ser. A **137**, 696 (1932).
[3] See, e.g., H. Nakamura, *Nonadiabatic Transition: Concepts, Basic Theories and Applications*, 1st ed. (World Scientific, Singapore, 2002).
[4] J. R. Rubbmark, M. M. Kash, M. G. Littman, and D. Kleppner, Phys. Rev. A **23**, 3107 (1981).
[5] A. Sibille, J. F. Palmier, and F. Laruelle, Phys. Rev. Lett. **80**, 4506 (1998).
[6] K. Mullen, E. Ben-Jacob, and Z. Schuss, Phys. Rev. Lett. **60**, 1097 (1988).
[7] See, e.g., S. N. Shevchenko, S. Ashhab, and F. Nori, Phys. Rep. **492**, 1 (2010).
[8] S. Longhi, Laser Photon. Rev. **3**, 243 (2009).
[9] A. Ruschhaupt, X. Chen, D. Alonso, and J. G. Muga, New J. Phys. **14**, 093040 (2012).
[10] X.-J. Lu, X. Chen, A. Ruschhaupt, D. Alonso, S. Guerin, and J. G. Muga, Phys. Rev. A **88**, 033406 (2013).
[11] R. Khomeriki and S. Ruffo, Phys. Rev. Lett. **94**, 113904 (2005).
[12] S. Longhi, J. Opt. B: Quantum Semiclassical Opt. **7**, L9 (2005).
[13] F. Dreisow, A. Szameit, M. Heinrich, S. Nolte, A. Tünnermann, M. Ornigotti, and S. Longhi, Phys. Rev. A **79**, 055802 (2009).
[14] M. Sillanpaa, T. Lehtinen, A. Paila, Y. Makhlin, and P. Hakonen, Phys. Rev. Lett. **96**, 187002 (2006).
[15] S. Longhi, Phys. Rev. E **73**, 026607 (2006).
[16] S. Longhi, Phys. Lett. A **359**, 166 (2006).
[17] S. Longhi, G. DellaValle, M. Ornigotti, and P. Laporta, Phys. Rev. B **76**, 201101(R) (2007).
[18] S. Longhi, Opt. Lett. **30**, 2781 (2005).
[19] S. Longhi, Phys. Rev. A **71**, 065801 (2005).

[20] G. Della Valle, M. Ornigotti, E. Cianci, V. Foglietti, P. Laporta, and S. Longhi, Phys. Rev. Lett. **98**, 263601 (2007).
[21] M. Ornigotti, G. Della Valle, D. Gatti, and S. Longhi, Phys. Rev. A **76**, 023833 (2007).
[22] S. Longhi, J. Phys. B: At., Mol. Opt. Phys. **40**, 4477 (2007).
[23] S.-Y. Tseng and M.-C. Wu, IEEE Photonics Technol. Lett. **22**, 1211 (2010).
[24] S.-Y. Tseng and M.-C. Wu, J. Lightwave Technol. **28**, 3529 (2010).
[25] S.-Y. Tseng, S. K. Choi, and B. Kippelen, Opt. Lett. **34**, 512 (2009).
[26] H. Liu and L. F. Wei, J. Lightwave Technol. **35**, 166 (2017).
[27] H. R. Lewis and W. B. Riesenfeld, J. Math. Phys. **10**, 1458 (1969).
[28] X. Chen, E. Torrontegui, and J. G. Muga, Phys. Rev. A **83**, 062116 (2011); Y. Ban, X. Chen, E. Y. Sherman, and J. G. Muga, Phys. Rev. Lett. **109**, 206602 (2012).
[29] S. Ashhab, J. R. Johansson, A. M. Zagoskin, and F. Nori, Phys. Rev. A **75**, 063414 (2007).
[30] A. V. Shytov, D. A. Ivanov, and M. V. Feigelman, Eur. Phys. J. B **36**, 263 (2003).
[31] W. D. Oliver, Y. Yu, J. C. Lee, K. K. Berggren, L. S. Levitov, and T. P. Orlando, Science **310**, 1653 (2005).
[32] C. M. Wilson, T. Duty, F. Persson, M. Sandberg, G. Johansson, and P. Delsing, Phys. Rev. Lett. **98**, 257003 (2007).

*Correction:* Two author names in Ref. [7] were misspelled and have been fixed.